01,13

Electrical resistivity and thermal conductivity of α-Zr at high pressures and high temperatures

© A.M. Molodets, A.A. Golyshev, A.S. Savinykh, G.V. Garkushin

Federal Research Center of Problems of Chemical Physics and Medicinal Chemistry RAS, Chernogolovka, Russia

E-mail: molodets@icp.ac.ru

Received July 15, 2024
Revised August 19, 2024
Accepted August 20, 2024

The article presents the results of measurements of the electrical resistance of α-Zr samples under shock compression conditions. Experiments with shock waves were accompanied by modeling the thermodynamic history of compression of samples and the synchronous history of changes in their electrical properties. Modeling of the electrophysical properties of α-Zr with its changes in volume and temperature under shock compression was carried out within the framework of a hydrocode containing equations of state and a semi-empirical zirconium resistivity model taking into account the saturation temperature. The free parameters of the semi-empirical model of the electrical resistivity of zirconium are determined. These parameters were also used to restore the temperature-baric dependence of the thermal conductivity of α-Zr at high pressures and temperatures.

Keywords: zirconium, shock waves, equations of state, electrical resistivity, resistivity saturation, thermal conductivity, high pressures.

DOI: 10.61011/PSS.2024.10.59630.193

1. Introduction

It is well known that zirconium has low cross-section of thermal neutrons trapping and high melting point. So, metallic zirconium and its alloys play important role in nuclear power industry. This metal is used (see [1]), to manufacture fuel rods, fuel clusters and other structures of nuclear reactors. When designing fuel rods we need to know the thermophysical characteristics of used materials, as such characteristics determine values of temperatures and type of temperature fields in structural elements, including fuel rods of the nuclear reactor. So, study of thermophysical properties and associated electrophysical characteristics of zirconium was under increased attention for long time period. In Ref. [2–4] analyzed and summarized the experimental material on temperature dependence of the electrical resistivity and thermal conductivity of zirconium at atmospheric pressure in temperature range up to thousands of degrees.

In cited papers the experimental data relating specific electrical resistivity and thermal conductivity of zirconium are presented by explicit functions of temperature only, i. e. evident dependence of thermophysical properties on volume in these functions is contained indirecttly. Currently works relating study of the volume-temperature or temperature-baric dependence of electro- and thermophysical properties of zirconium are not numerous [5–7]. At the same time, it seems that such studies are expedient rom both applied and fundamental points of view. The applied expediency is associated with risks of emergency effect which is accompanied by heating and compression-tension of structures comprising zirconium. From physical point of few data on volume-temperature dependence of electro- and thermophysical properties of this metal are important in objectives of modeling the thermal processes in reactors under standard and non-standard loads.

In this context this paper task is experimental-calculation reconstruction of volume-temperature dependence of the specific electrical resistivity of allotropic modification of zirconium with hexagonal close-packed lattice (α-Zr) in range of high pressures and temperatures. In paper technique and methods [8] of measurement and modeling of thermophysical properties of compressed and heated metallic samples under conditions of step-type shock-wave compression.

2. Samples, shock-wave loading and registration of electrical resistance of shock-compressed samples of zirconium

2.1. Samples

Samples are prepared from rod of iodide zirconium with diameter ~ 20 mm, containing (as per TU 95.6−97) 99.999% zirconium. The rod comprises single-crystal grains of zirconium with size 3−5 mm of hexagonal close-packed phase α-Zr. Disk 0.5 mm thick was cut perpendicular to axis of rod in electrical discharge machine. From disk a strip 20 mm long and ~ 3 mm wide was prepared, in steel rollers it was transformed in tape $\sim 0.04-0.05$ mm thick and ~ 4.4 mm wide. Then this tape was cut to sections 25 mm long and ~ 2 mm wide, and studied samples of tape form

were formed from them. Current conductor in form of strips of copper foil 0.015 mm thick were spot welded to ends of the tape sample. The zirconium sample with conductors was a metering cell, which plane located in parallel to front of shock wave. The measured electrical resistivity of prepared zirconium samples was $\rho_0 = 51(2)\,\mu\Omega \cdot$ cm. Initial electrical resistivities R_0 of tape zirconium samples were measured for each experiment and were within range $R_0 = 1.4-1.6\,\Omega$.

2.2. Generator of step-like shock-wave loading

Figure 1 presents scheme of used explosion generator of shock-wave loading. Metal flat impactor *1* is accelerated by explosion products to speed W_0. The target is shock anvils made of two „rigid" metal plates *2* and *4*, between them „soft" layer of insulator *3* is located. Insulator *3* is set of teflon films glued with vacuum lubricant. Vacuum lubricant of Russian origin (TU 38.401-58-172-96) was used. The teflon films 0.1−0.5 mm thick are industrial teflon films (fluoroplastic tape F-4 GOST 24222-80 „PN" — spacing nondirectional). Plates *2* and *4* are made of steel (steel 12Kh18N10T, hereinafter steel Kh18) or tungsten. Thin (as compared to insulator thickness) sample under study *5* is located in the insulator *3* at distance h_1 from *2* and h_2 from *4*. Thicknesses h_1 and h_2 are varied by set of teflon films glued by micron layers of vacuum lubricant.

Operation of the generator of step-like shock-wave loading is explained in Figure 2. Here arrow with symbol D designates (see Figure 2, *a*) the trajectory of single shock wave formed after collision of the impactor and plate *2*. At time t_0 the gap is breaking at interface metal *2*−teflon *3*, then in insulator *3* the first shock wave spreads with speed D_1 and with pressure after its front P_1 (see Figure 2, *b*). At time t_1 of wave D_1 arrival on sample *5* the reverberation of compression and unloading waves starts in it. The reverberation runs for time period δ_1 and finishes when pressure P_1 is achieved in sample. Then, at time t_r, wave D_1 is reflected from the plate *4* in form

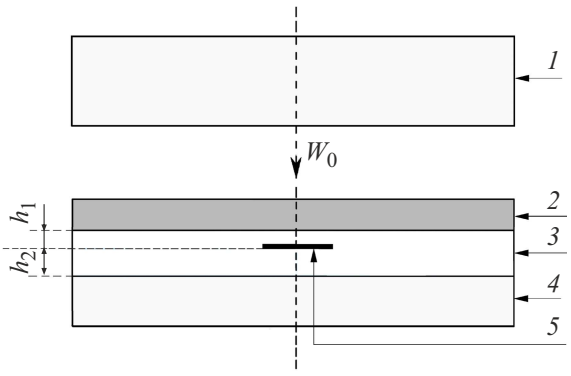

Figure 1. Generator of step-like shock-wave loading. *1* — aluminium impactor, *2* — steel or tungsten plate, *3* — teflon, *4* — steel or tungsten plate, *5* — tape sample $h_0 = 0.045(5)$ mm thick and $a_0 = 1.90(5)$ mm wide.

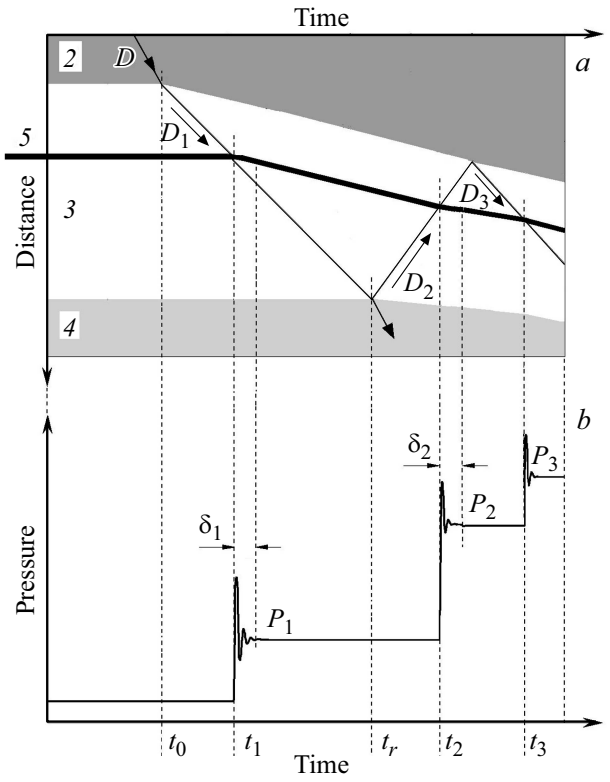

Figure 2. Operation of generator of step-like cyclic shock loading. (*a*) Kinematics of shock waves in coordinates Distance−Time, symbols *2, 3, 4, 5* mean same as in Figure 1. (*b*) Profile (dependence on time) of pressure in sample under study. Symbols in Figure 2, *b* are explained in text.

of second compression wave D_2. Wave D_2 stimulates same reverberation of compression and unloading waves in sample during time period δ_2, it finishes by creation in sample of second pressure step P_2. Further, after formation of reflected wave D_3, the third step with pressure P_3 is formed etc. Note that period τ_0 of cyclic component is determined by value about $\tau_0 \sim 2h_0/C_0$, where h_0 — sample thickness, C_0 — sound speed in sample material. At typical values for metal samples $h_0 \sim 0.05$ mm and $C_0 \sim 5$ mm/mks τ_0 is $\tau_0 \sim 0.02$ mks.

Thus, used generator stimulates in the sample under study the step-like cyclic loading mode, characterized by amplitudes of steps P_1, P_2, P_3 and cyclic component of pressure δ on front of each step.

Value of pressures P_1, P_2, P_3 varies with speed of impactor *1* and material of plates *2, 3, 4* (see Figure 1). This paper presents two series of explosion experiments which differ by plate material and their thickness. These parameters for each series are selected such that on one hand pressures P_1 in first step were different, and at same time did not exceed pressure of polymorphic transformation of zirconium during shock-wave loading. But at same time sets of parameters are were formed such that pressures P_2 of second step in both series deliberately stimulated the polymorphic transition of zirconium samples.

Table 1. Parameters of generators of step-like shock-wave loading

Plate	*1*			*2*		*3*		*4*	
	W_0, km/s	Metal	H_1, mm	Metal	H_2, mm	h_1, mm	h_2, mm	Metal	H_4, mm
Series *I*	1.20	Al	7.0	W	1.42	0.66	0.56	W	1.44
Series *II*	1.30	Al	7.0	X18	1.96	0.66	1.30	X18	3.26

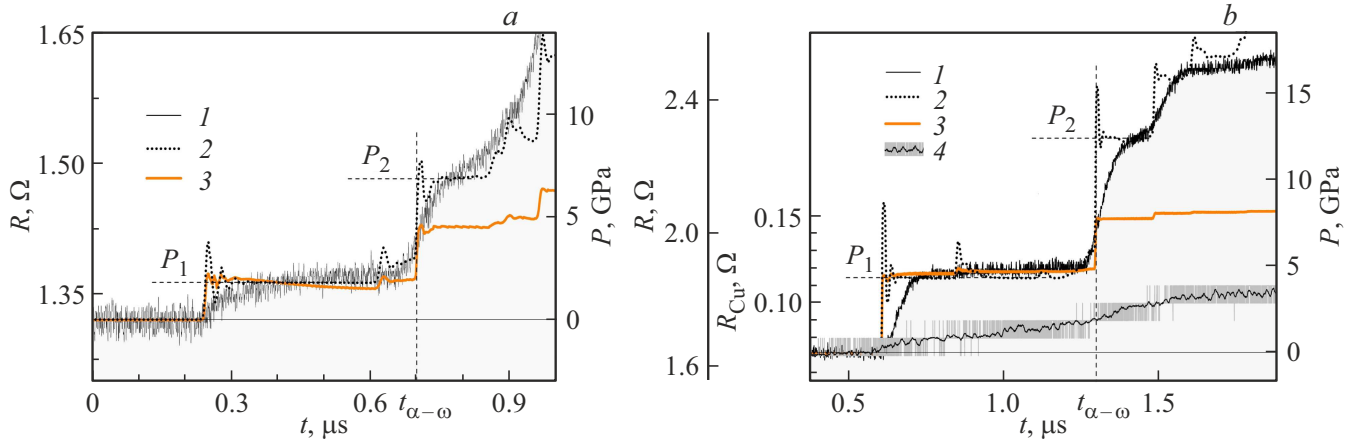

Figure 3. Electrical resistance and pressure during step-like shock compression of zirconium samples. *1* — experimental profiles of electrical resistance of zirconium samples, *2* — model profiles of pressure, *3* — synchronous model profiles of electrical resistance of samples, *4* — experimental profile of electrical resistance $R_{Cu} = R_{Cu}(t)$ of „copper" cell. Time $t_{\alpha-\omega}$ designates start of polymorphous α-Zr $\rightarrow$ ω-Zr transition of zirconium. (*a*) Results for first series. (*b*) Results for second series. Axes of ordinates R for *1, 3*, and R_{Cu} for *4* are located to the left, for *2* — axis of ordinates is located to the right.

Table 1 presents sets of parameters of generators for each series. Numeration of first line in Table corresponds to same in Figure 1; H_1, H_2, h_1, h_2, H_4 — thicknesses of plates *1*, *2* ÷ *4*.

2.3. Measurement of electrical resistance of shock-compressed samples of zirconium

During measurement of electrical resistance of shock-compressed sample the capacitor 1000 μF was used, it discharges via resistor 100 Ohm. As a result during time of registration ($\sim 2\,\mu$s) along tape sample practically constant current flows $J_0 = 3.0(1)$ A. The electrical resistance of sample was measured as per two-point scheme using Wheatstone bridge. In experiment the we measured profile (dependence on time t) of voltage change of unbalanced bridge $\Delta U = \Delta U(t)$. Profiles $\Delta U(t)$ were measured by high-frequency oscilloscope Tektronix DPO4104B. Profiles of resistance $R = R(t)$ were determined as sum $R = R_0 + k\Delta U$, where R_0 initial electrical resistance of sample, k preliminary determined calibration coefficient. Value of complicating effects of shunting, skin effect, heat exchange of thin metal samples with the surrounding insulator are considered in [8].

Typical experimental oscillograms $R = R(t)$ in form of profiles of electrical resistance *1* of zirconium samples in first and second series are presented in Figure 3, *a* and Figure 3, *b*, respectively.

In experiments also synchronous profiles $R_{Cu} = R_{Cu}(t)$ of electrical resistance of „copper" metering cell were measured, in cell the zirconium sample was replaced by copper analogue. In Figure 3, *b* profile *4* presents the typical oscillogram of „copper" cell. From Figure 3, *b* we see that at pressure P_1 value of electrical resistance of copper analogue together with current conductors is by order of magnitude lower the effective signal *1*. Based on this the change in electrical resistance of copper current conductors was not further considered.

3. Modeling of thermodynamic state and volume-temperature dependence of electrical resistivity of zirconium

The electrophysical properties of zirconium at high pressures under conditions of step-like shock compression were reconstructed as result of joint modeling of thermodynamic state of zirconium during shock compression and synchronous effects of its electrical resistivity change with change in volume and temperature.

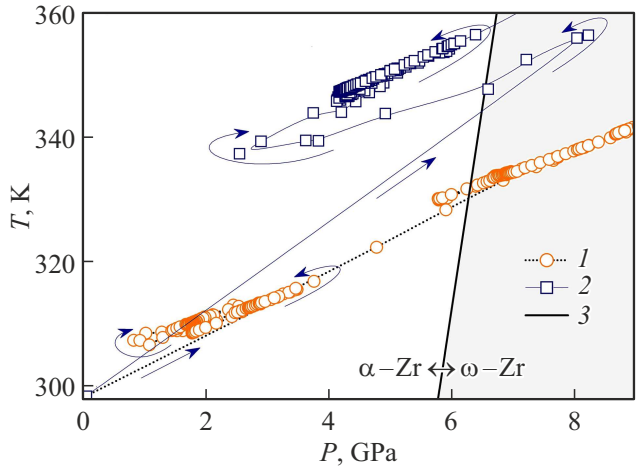

Figure 4. Phase trajectories of step-like cyclic shock compression in coordinates pressure P – temperature T. *1* and *2* — phase trajectory of zirconium compression on first step in experiments of first and second series, respectively, arrows designate sequences TP of stets of zirconium α-Zr in time at step-like cyclic shock compression. *3* line of polymorphic α-Zr $\rightarrow$ ω-Zr transition of zirconium during shock compression plotted as per results in [14].

3.1. Modeling of thermodynamic state

Modeling of thermodynamic state of zirconium samples in performed experiments was performed in program (hydrocode) STAG for PC [9], based on previously developed equations of state. The equations of state for α-Zr are taken from [10]. references to papers with equations of state of rest materials are in [11,12].

Program STAG ensures calculation of wave interactions and thermodynamic state in form of profiles of pressure, temperature and specific volume for any Lagrangian particle of each layer of multilayer target of explosion generator during one-dimensional dynamic loading. As width of the tape zirconium sample a_0 by order of magnitude exceeds its thickness h_0, then in hydrocode the zirconium sample was modeled by plate with initial thickness h_0. Therefore, in work the calculation profiles of pressure $P(t)$, temperature $T(t)$ and specific volume $V(t)$ for Lagrangian coordinate $h_0/2$ of zirconium late were accepted. Figure 3 shows model profiles *2* of pressure $P(t)$ for both series.

As per Figure 3 pressure P_1 in sample of iodide zirconium is about $\sim 2-5$ GPa. The dynamic yield limit of pure zirconium, determined as per experimental results [13] is much lower 0.38 GPa, this justifies the use of hydrodynamic approximation during numerical modeling of the experiment. Correct use of hydrodynamic approximation for modeling of performed experiments is discussed in Section 6. On other hand, note that pressures in our experiments were rather low to neglect the electronic component in equations of state of zirconium and limited only by photonic contribution into free energy of metal. In such approximation the equations of state for α-Zr from [10] are given in Section 5.

Time exclusion from the calculation profiles $P(t)$ and $T(t)$ provides phase trajectory in coordinates pressure-temperature in each experiment. Figure 4 by graphs *1* and *2* shows the phase trajectories of step-like cyclic compression in experiments of first and second series, respectively. Figure 4 shows that during material compression its temperature covers wide range 305–360 K. This effect is due heating during reverberation of waves in rigid sample surrounded by soft insulator during step-like cyclic compression.

Note that the „reverberation“ heating of the sample, which takes place in the experiments carried out, is not usually considered, but plays an important role in our modeling of the electrophysical properties of shock-compressed samples.

Thus, calculations of temperatures and pressures determine the studied region α-Zr in range of temperatures $\sim$ 305–360 K and pressures $\sim 2-5$ GPa.

3.2. Modeling of electrical resistivity of shock-compressed samples

As model of volume (V) — temperature (T) dependence of electrical resistivity $\rho = \rho(V,T) \propto \rho_0 \varphi \epsilon$ we used relationship in form of product of initial electrical resistivity ρ_0 and two functions: volume component $\varphi = \varphi(V)$ and temperature component $\epsilon = \epsilon(T)$.

View of $\varphi = \varphi(V)$ is taken from [8,15]

$$\varphi = \left(\frac{V}{V_0}\right)^{n/3} \left(\frac{\upsilon_0 - V}{\upsilon_0 - V_0}\right)^{-2n}, \qquad (1)$$

where according to [8] the specific volume V_0 at room temperature and atmospheric pressure, and parameter υ_0 are assumes known parameters of equations of state (for α-Zr see [10] and Table 3 in Section 5), n dimensionless adjusting coefficient. According to prototype [15] value of coefficient n is determined by the mechanism pf conduction electrons scattering in metals. For example, value $n = 2$ is typical for model of free electrons in ideal metal, $n = 3$ is expected for $s-d$ scattering of electrons.

As temperature component of the electrical resistivity previously in [8] exponential function in form $\epsilon = \epsilon(T) = \left(\frac{T}{T_0}\right)^{\alpha}$ with constant adjusting coefficient α was engaged. But, high-temperature isobar of electrical resistivity of zirconium is curve with saturation temperature (see [2,3]). Due to this for the temperature component of zirconium the empirical dependence $\epsilon = \epsilon(T)$ in form of exponential function was taken

$$\epsilon = \frac{x}{\exp(x) - 1}, \qquad (2)$$

where $x = \theta_\epsilon / T$, θ_ϵ — adjusting coefficient with temperature dimension.

Table 2. Individual coefficients of model functions (3) and (6) for α-Zr

n	V_0, cm^3/mol	υ_0, cm^3/mol	θ_ϵ, K	ϵ_0	$\rho_0, \mu\Omega \cdot$ cm	k_{0l}, W/(mK)
2.65	14.022	60.596	700.0	0.2481	43.3	7.0

So, model relationship for electrical resistivity $\rho = \rho(V, T)$ of the considered metal is as follows

$$\rho = \rho_0 \left(\frac{\epsilon}{\epsilon_0}\right) \varphi, \tag{3}$$

where $\rho_0 = \rho(T_0, V_0)$ — electrical resistivity of material at temperature T_0 and volume V_0, $\epsilon_0 = \epsilon(T_0, V_0)$.

Thus, the relationships (1)−(3) shall identify the electrophysical properties of metal by its experimental value ρ_0 and by two adjustable parameters θ_ϵ, n. Values ρ_0, θ_ϵ, n for α-Zr were determined as follows.

Values ρ_0 provided by various authors at $T_0 = 298$ K and atmospheric pressure $P_0 = 1$ atm for zirconium are in range $40-50\,\mu\Omega \cdot$ cm (see [3]). This range also includes values for our samples $\rho_0 = 51(2)\,\mu\Omega \cdot$ cm. At the same time in [3] it was recommended to use value $\rho_0(T_0, P_0) = 43.3\,\mu\Omega \cdot$ cm. Due to this as unchanged parameter of the model function (3) for α-Zr value $\rho_0 = 43.3\,\mu\Omega \cdot$ cm was taken.

The adjustable parameters θ_ϵ, n for α-Zr were determined by joint adjustment for static experimental data [3,4] and experimental data obtained in the presented paper, considering in both cases its volume-temperature dependence of electrical resistivity. Algorithm of constants n and θ_ϵ selection for α-Zr is as follows.

Note that relationship (3) ensures formation of the expression for electrical resistance R of sample of considered material under conditions of flat one-dimensional compression

$$R = R_0 \left(\frac{\epsilon}{\epsilon_0}\right) \left(\frac{V_0}{V}\right) \varphi, \tag{4}$$

where R_0 — initial electrical resistance of sample at room temperature T_0 and atmospheric pressure P_0, multiplier (V_0/V) considers change in thickness of flat sample during flat one-dimensional deformation.

Substitution of model profiles of temperature $T = T(t)$ and volume $V = V(t)$ in (4), provided the model profile $R_m = R_m(t)$, which can be adjusted to the experimental profile $R = R(t)$ of electrical resistance by selecting coefficients n and θ_ϵ.

As zero approximation for n we take $n = 2$. Zero approximation for $\theta_\epsilon = 721$ K was obtained as result of function (3) adjustment to experimental data from [3] under condition $\varphi = \text{const} = 1$. The first iteration of profile $R_m = R_m(t)$ was made by n variation to value $n = 2.6$ at constant value θ_ϵ. Then, value $\theta\epsilon$ varied at $n = 2.6$ to value $\theta_\epsilon = 710$ K, ensuring coincidence of model isobar of electrical resistivity α-Zr and experimental isobar from [3] considering change in volume of zirconium according to its equation of state. Finally, values $R_m = R_m(t)$ and $R = R(t)$ are compared at pressure P_1, $n = 2.6$ and $\theta_\epsilon = 710$ K. If profiles $R_m = R_m(t)$ and $R = R(t)$ differ by more than 1%, the cycle was repeated. As a result of further iterations the final optimal values of required parameters were determined, they were practically same for both series.

These values are listed in Table 2.

The model profiles with determined parameters are presented by graphs *3* in Figure 3. We see that first steps of model profiles $R_m = R_m(t)$ coincide with the experimental profiles $R = R(t)$ with accuracy to 1%.

Note that pressures P_1 (see Figure 3) on first step until time $t_{\alpha-\omega}$ are located in the phase diagram of zirconium to the left from line 3 of polymorphic transformation α-Zr → ω-Zr in Figure 4. This means that in performed experiments the measured electrical resistivities until time $t_{\alpha-\omega}$ belong to polymorphous modification α-Zr. Note also that model profiles of electrical resistance *3* in Figure 3 at times of modification ω-Zr existence at $t > t_{\alpha-\omega}$ relate to metastable α-Zr, and thus significantly differ from the experimental profiles of the electrical resistance *1* in Figure 3.

Finally note, that as per this logic the joint analysis of experimental profiles of the electrical resistivity *1* and model profiles *2* and *3* in Figure 3 ensures evaluation of pressure P_{tr} of polymorphic transformation α-Zr → ω-Zr in studied samples during their shock-wave loading. Actually, Figure 3, *a* ensures evaluation from top as $P_{tr} < P_2 = 6.9$ GPa. On other hand, Figure 3, *b* ensures evaluation from bottom as $P_{tr} > P_1 = 4.3$ GPa. As a result the summary evaluation of pressure of polymorphic transformation is expressed as $P_{tr} = 5.6$ GPa (1.3). It is seen that obtained value does not conflict with line *3* Figure 4 for the polymorphic α-Zr → ω-Zr transition of zirconium during shock compression, this line was plotted as per results of [14].

Thus, presented experimental and calculation method ensures determination of values of parameters n and θ_ϵ for reconstruction of volume-temperature dependence of electrical resistivity $\rho = \rho(V, T)$ for α-Zr in form (3) under dynamic pressures $\sim 2-5$ GPa and temperatures $\sim 305-360$ K.

4. Discussion of results

It is well known that plastic deformation of metals during shock compression facilitates creation of the defects that irreversibly change the electrical resistivity of metals during the process of their deformation. But in relationships (1)−(3) we assume that volume-temperature change in electrical resistivity of shock-compressed zirconium is reversible and prevails over the irreversible change in its

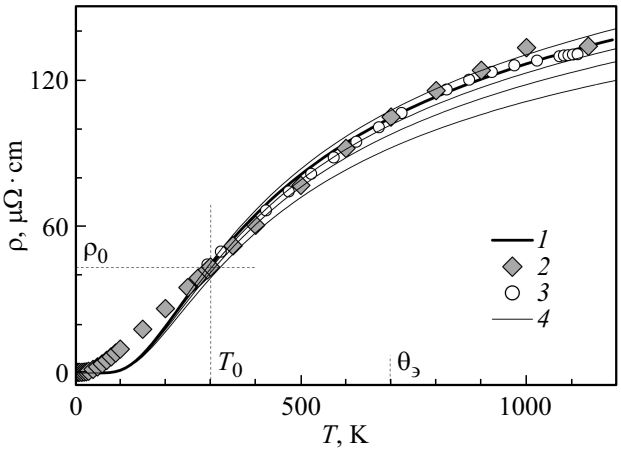

Figure 5. High-temperature isobars of electrical resistivity α-Zr. *1* — model atmospheric isobar $\rho = \rho(V, T)$. *2* — recommended experimental values for atmospheric isobar from [2]. *3* — recommended experimental values from [3]. *4* — model isobars of electrical resistivity of zirconium under pressures (from top down) -1.0, 1.0, 2.5 and 5.0 GPa.

electrical resistivity. Due to this point of view we can suppose that determined parameters n and θ_ϵ, relating to the shock-compressed zirconium, will be with acceptable efficiency to zirconium under static conditions where plastic deformation is absent. Review of the below Figures 5 and 6 justifies this supposition.

Thus, Figure 5 presents volume-temperature dependence *1* of electrical resistivity α-Zr along atmospheric isobar plotted using (3), reference value $\rho_0 = 43.3\,\mu\Omega \cdot$ cm from [2] and values n, ϵ_0 and θ_ϵ, from Table 2. Here the recommended values of electrical resistivity *2* from [2] of polycrystalline zirconium with purity 99.95%, and similar data *3* from [3] are presented.

It is seen in Figure 5, that in temperature range 300–1100 K the derivative with respect to temperature of model curve *1* decreases with temperature and practically coincides with static experimental data *2* and *3*. At decreased temperatures, in range $T < T_0$ K the model curve is located significantly lower the experiment [2]. Anyway qualitatively the model curve *1* here also agrees with [2]. Actually, in cryogenic temperature range $T \sim 1$–200 K the derivative with respect to temperature of the model curve *1* in agreement with experiment [2] increases with temperature.

Agreement between the model result *1* and experiment *2* and *3* justifies the forecast of isobars of electrical resistivity α-Zr at high, including negative (tension) pressures. This forecast is presented by graphs *4* in Figure 5.

Let's discuss now the use of volume-temperature dependence of electrical resistivity of zirconium for calculation of its thermal conductivity at high temperatures and pressures. In Figure 6 graph *1* represents the electronic component of thermal conductivity of zirconium samples k_e, calculated as per Wiedemann–Franz law $k_e = k_e(V, T) = LT/\rho$ with theoretical value of Lorentz number $L = 2.45 \cdot 10^{-8}\,\mathrm{W\Omega/K^2}$ and ratio (3) for α-Zr. Figure 6 also presents graph *2* being generalization of the literature experimental data in thermal conductivity of zirconium from [4] in form of empirical polynomial.

$$k_{\exp} = 8.8527 + 7.0820 \cdot 10^{-3}T + 2.5329 \cdot 10^{-6}T^2 + 2.9918 \cdot 10^{3}T^{-1} \quad (5)$$

We see that the model graph *1* is located by about 25% lower the experimental values of thermal conductivity of zirconium *2*. Frequently for zirconium (see references in [3]) smoothing of this difference is achieved by temperature dependence of Lorentz number at level $L = (3.1 \cdot 10^{-8} - 3.5) \cdot 10^{-8}\,\mathrm{W\Omega/K^2}$. But in the previous paper it was possible to agree *1* and *2* at single theoretical value L. Actually, supposing similar to [16] that difference between *1* and *2* entirely is due contribution of the lattice thermal conductivity k_l, we write the expression for volume-temperature dependence of thermal conductivity of zirconium $k = k(V, T)$ as sum

$$k = k_e + k_l, \quad (6)$$

where, like above, $k_e = LT/\rho$ is the electronic component of thermal conductivity calculated as per Wiedemann–Franz law with $L = \mathrm{const} = 2.45 \cdot 10^{-8}\,\mathrm{W\Omega/K^2}$, and second term is Dugdal–Macdonald model expression of volume-temperature dependence of lattice thermal conductivity $k_l = k_l(V, T)$

$$k_l = k_{0l}\left(\frac{T_0}{T}\right)\left(\frac{V}{V_0}\right)\left(\frac{\Theta}{\Theta_0}\right)^3\left(\frac{\gamma_0}{\gamma}\right)^2. \quad (7)$$

Functions $\Theta = \Theta(V)$ and $\gamma = \gamma(V)$ in (6) are determined (see details in [16] for iron) by relationships (9) and (11)

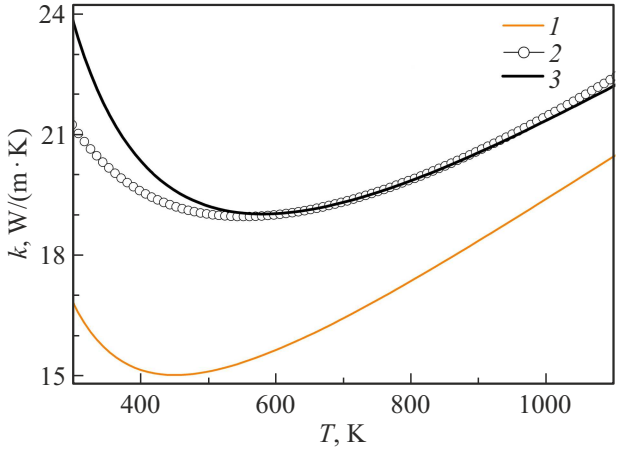

Figure 6. Thermal conductivity k of zirconium α-Zr vs. temperature T along atmospheric isobar. *1* — electronic component k_e. *2* — generalization of experimental isobars of thermal conductivity at atmospheric pressure (5) from [4]. *3* — sum of electronic and lattice components $k = k(V, T) = k_e + k_l$ (6).

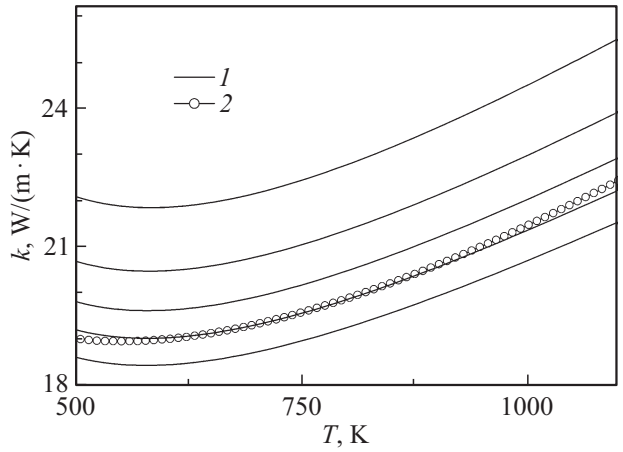

Figure 7. Temperature-baric dependence of thermal conductivity α-Zr at high temperatures and pressures. *1* — model isobars of thermal conductivity at pressure (from bottom to top) −1.0, 0.0, 1.0, 2.5, 5.0 GPa. *2* — fragment of graph (5) generalizing experimental isobars of thermal conductivity at atmospheric pressure from [4].

from next Section 5 describing the thermal equation of state α-Zr. Parameter k_{0l} is adjustable parameter intended to agree the model calculations (6) with the experiment (5) from [4].

In Figure 6 graph 3 represents calculation of $k = k(V, T)$ as per (6) along atmospheric isobar with value of parameter $k_{0l} = 7.0\,\mathrm{W/(m \cdot K)}$. It is seen that in temperature range 500−1100 K the model calculations *3*, considering the equation of state of zirconium, coincide with generalizing experimental data *2* from [4]. As the temperature decreases in range 300−500 K graphs *2* and *3* difference occurs. But, note that even at temperature 300 K this difference does not exceed standard deviation for (5) from [4].

Similar to forecast for electrical resistivity the forecast of isobars of thermal conductivity α-Zr was made at high, including tension pressures. This forecast is presented by graphs *1* in Figure 7. It is seen that, for example, at temperature $T = 750\,\mathrm{K}$ the effect of pressure action on thermal conductivity coefficient α-Zr is 0.58 W/(mK) per 1 GPa.

So, model (6), based on the experimental-calculated data on electrical resistivity and semiempirical equations of state, is in agreement with the experimental data on volume-temperature dependence of the thermal conductivity coefficient α-Zr in temperature range 500−1100 K at atmospheric pressure. The model ensures also evaluation of change in thermal conductivity coefficient under action of compression and tension pressures in range of −1 GPa to +5 GPa.

5. Thermal equation of state α-Zr

Used here thermal equation of state (pressure $P = P(V, T)$ dependence of specific volume V and temperature T) for α-Zr from [10] looks like:

$$P = 3R\Theta\frac{\gamma}{V}\left(\frac{1}{2} + \frac{1}{\exp(\Theta/T) - 1}\right) + P_x, \qquad (8)$$

where R — specific gas constant, key functions $\Theta = \Theta(V)$, $\gamma = \gamma(V)$ and $P_x = P_x(V)$ are algebraic volume functions. So, characteristic temperature $\Theta = \Theta(V)$ is expressed as

$$\Theta = \Theta_0\left(\frac{\upsilon_0 - V}{\upsilon_0 - V_0}\right)^2\left(\frac{V_0}{V}\right)^{2/3}, \qquad (9)$$

where

$$\upsilon_0 = V_0\left(1 + \frac{2}{\gamma_0 - 2/3}\right). \qquad (10)$$

In (9) the parameter Θ_0 is initial value of characteristic temperature $\Theta_0 = \Theta(V_0)$ at initial specific volume V_0, initial room temperature $T_0 = 298.15\,\mathrm{K}$ and initial atmospheric pressure. The parameter υ_0 is expressed via V_0 and Gruneisen thermodynamic parameter $\gamma_0 = \gamma_0(V_0, T_0)$. The volume dependence of Gruneisen coefficient $\gamma = \gamma(V)$ and potential pressure $P_x = P_x(V)$ looks like

$$\gamma = -\frac{d\ln\Theta}{d\ln V} = \frac{2}{3} + \frac{2V}{\upsilon_0 - V}, \qquad (11)$$

$$P_x = 3C_1x^{1/3}\left(-\frac{1}{5}x^{-2} + 2x^{-1} + 6 - x + \frac{1}{7}x^2\right) + C_2. \qquad (12)$$

$$x = V/\upsilon_x. \qquad (13)$$

Set of determining parameters Θ_0, V_0, υ_0, υ_x, C_1, C_2 for (8)−(13) and their numerical values from [10] are presented in Table 3.

6. Verification of model of step-like cyclic compression of zirconium samples

It was mentioned above that accounting of „reverberation", step-like cyclic mode plays important role in modeling the electrophysical properties of shock compressed samples. In this relation the experiments were performed (see scheme in Figure 8), their task was to confirm compliance of made modeling of behaviour of zirconium of submillimeter thickness in enclosed by soft insulator during its step-like cyclic compression.

In Figure 8 scheme in Figure 1 is actually presented, in it analogue of first metal plate is copper impactor, and second metal plate is absent. Therefore operation of generator in Figure 8 is explained by evolution of compression waves in Figure 2 until t_r.

So, in Figure 8 flat copper impactor *1*, accelerated in the pneumatic gun to speed W_a, collides with transparent plexiglass insulator *2*, inside which the thin plate zirconium sample is located *3*. Thicknesses of impactor, insulator and sample limited the mode of single-step compression

Table 3. Parameters of thermal equation of state (8) for α-Zr

Θ_0, K	V_0, cm^3/mol	υ_0, cm^3/mol	υ_x, cm^3/mol	C_1, GPa	C_2, GPa
217.5	14.022	60.596	37.859	−111.1710	2296.4979

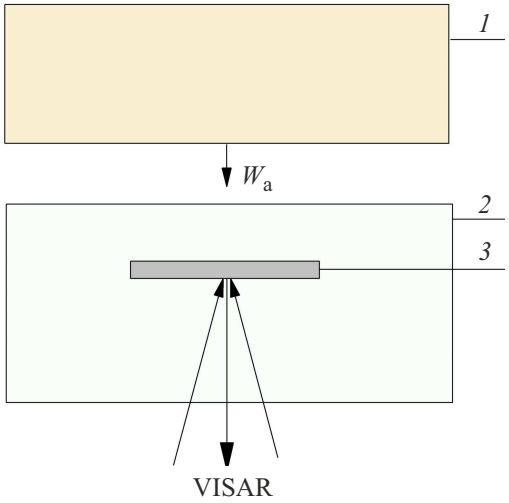

Figure 8. Scheme of experiment on recording the profile $u(t)$ (dependence on time t) of mass speed of frontal surface of sample. *1* — copper impactor with diameter 48.0 mm and thickness 2.5 mm flying at speed $W_a = 347$ m/s, *2* — plexiglass block with diameter 50 mm and thickness ~ 10 mm, *3* — zirconium sample ~ 20 mm in diameter and $h_0 = 0.20$ mm thick, rare surface of sample is at distance 2.0 mm from rare surface of block *2*.

to pressure P_1 with high-frequency cyclic component which was consistently represented *in situ* in form of submicrosecond pulsation of mass speed $u(t)$ of frontal surface of submillimeter sample. Profile $u(t)$ was measured using precision optical method VISAR [17]. The used laser method ensured speed measurement with accuracy ± 3 m/s and time resolution 2 ns maximum, light spot diameter of laser on the studied surface did not exceed 0.5 mm. One of three practically coinciding experimental profiles $u(t)$ is presented in Figure 9, *a* by graph *1*. We see that profile *1* in Figure 9, *a* contains pulsations with period $\Delta\tau$, which unambiguously indicate the circulation of stress waves in the compressed sample, i. e. cyclic mode of sample compression in this experiment. Note that value $\Delta\tau$ ensures calculation of speed of perturbations spreading C in compressed sample by dividing its double thickness $2h_0$ by$\Delta\tau$ as $C = 2h_0/\Delta\tau$. If we then compare this value with the volume $C_0 = 3.83$ km/s and longitudinal $C_l = 4.684(6)$ km/s speeds of sound in zirconium E100 from [13], then in case $C = C_0$ we can assume that used above hydrodynamic approximation is true. Option $C = C_l$ means noticeable elastic-plastic effects in zirconium sample under conditions of performed experiment. It turned out that mean arithmetic value C for two first pulsations gives value $C = 4.75(20)$ km/s, this practically coincides with C_l and, therefore, under conditions of performed experiments with zirconium samples the elastic-plastic effects play their role. In this relation the differences in results of hydrodynamic approximation use and calculation results were reviewed considering the elastic-plastic effects in α-Zr.

Evaluation of differences in modeling, when using hydrodynamic approximation and elastic-plastic model, was performed as follows. Two sets of profiles of mass speed of frontal surface of sample $u_{mod}(t)$ were calculated, ans also stress profile $Sx(t)$ and pressure profile $P(t)$ for Lagrangian coordinate $h_0/2$ of sample. In first set the elastic-plastic model with dynamic yield strength $G_\tau = 0.38$ GPa was used, in second set the hydrodynamic approximation was used, where $\sigma_\tau = 0$ GPa. Appropriate model profiles are presented in Figures 9, *a* and 9, *b*.

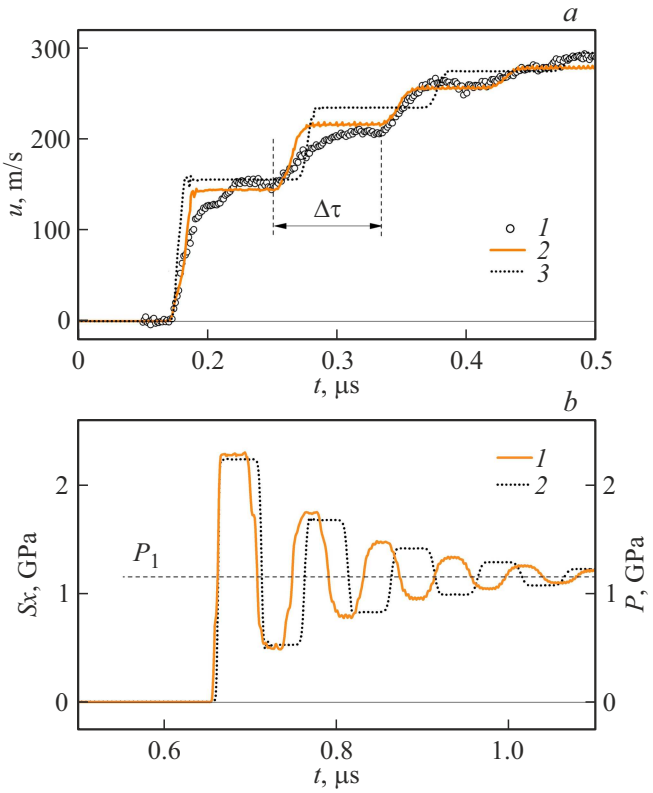

Figure 9. Profiles of mass speed of frontal surface of sample and stress in middle of sample. (*a*) *1* — experimental profile $u(t)$ (diameter of dot-circle *1* is 6 m/s in speed and 4 ns in time), *2* — model profile $u_{mod}(t)$ within the framework of elastic-plastic model, *3* — model profile $u_{mod}(t)$ in hydrodynamic approximation. (*b*) *1* — model profile of stress $S_x(t)$ within framework of elastic-plastic model, *2* — model profile of pressure $P(t)$ in hydrodynamic approximation. P_1 — pressure similar in meaning to pressure P_1 in profiles *2* Figure 3.

It is seen in Figure 9, *a* the pulsation period of model profile *2* practically coincides with $\Delta\tau$, at the same time the pulsation period of profile *3* exceeds $\Delta\tau$. Also amplitudes of profile steps *2* are located to the experiment *1* closer then steps of profile *3*. But note that all three profiles move closer after $\sim 0.3\,\mu$s. Similarly amplitudes of model profiles *1* and *2* move closer, in the effort to reach same value P_1, as we see in Figure 9, *b*. Note also that, as it is known, the plastic deformation does not change value of metal volume. So, we can say that results of model calculations of electrical resistance of thin samples of zirconium in the hydrodynamic approximation and considering elastic-plastic behaviour α-Zr practically coincide between each other after $\sim 0.3\,\mu$s from start of step-like cyclic compression phase.

In general, the equality of the volume of metal together with the equality of pressures and mass speeds when modeling the first step P_1 in hydrodynamic and elastic-plastic justifies the correctness of use of hydrodynamic approximation to model the experimental data obtained in this paper.

7. Conclusion

The electrical resistivities of samples α-Zr are measured in conditions of step-like cyclic shock compression in temperature range $\sim 305-360$ K and pressure range $\sim 2-5$ GPa.

Model of step-like cyclic shock compression of thin rigid sample enclosed by soft insulator is verified.

The semiempirical mode of volume-temperature dependence of electrical resistivity of zirconium with saturation temperature is developed, and values of free parameters of this model for α-Zr in pressure range $2-5$ GPa and temperature range $300-1100$ K are identified.

Corresponding to the experiment description of volume-temperature dependence of thermal conductivity coefficient α-Zr at high temperatures is formulated using equations of state of zirconium, Wiedemann–Franz law with theoretical Lorentz number and Dugdal–Macdonald model relationship.

In temperature range $500-1100$ K and pressure range of -1 GPa to $+5$ GPa the temperature-baric dependence of electrical resistivity, and thermal conductivity coefficient α-Zr, is made, it is 0.58 W/(mK) per 1 GPa.

Funding

Results are obtained within framework of Contract No. 1770641334821000138O/22398/90 „Experimental study of thermophysical, strength properties of materials of nuclear power industry and properties of shock compressed plasma. Stage 2023–2024“, performed within the framework of complex program „Development of equipment, technologies and scientific researches in the field of atomic nuclear energy use in the Russian Federation“ for the period up to 2024, and under State Assignment No. 124020600049-8.

Conflict of interest

The authors declare that they have no conflict of interest.

References

[1] V.I. Deev, N.V. Shchukin, A.L. Cherezov. Osnovy rascheta sudovykh YaEU / Pod redaktsiej prof. V.I. Deev. NIYaU MIFI, M. (2012). 256 s. (in Russian).
[2] P.D. Desai, H.M. James, C.Y. Ho. Journal of Physical and Chemical Reference Data, **13**, *4*, 1097 (1984).
[3] N.D. Milosevic, K.D. Maglic. International Journal of Thermophysics, **27**, *4*, 1140 (2006).
[4] J.K. Fink, L. Leibowitz. Journal of Nuclear Materials **226**, 44 (1995).
[5] Y. Tange, E. Takahashi, Ken-ichi Funakoshi. High Pressure Research *31*, *3*, 413 (2011).
[6] P.S. Balog, R.A. Secco J. Phys.: Condens. Matter **11**, 1273–1287 (1999).
[7] I.C. Ezenwa, T. Yoshino. Phys. Status Solidi B **260**, 2300079 (2023).
[8] A.M. Molodets, A.A. Golyshev. Fizika Zemli, **4**, 39 (2024). (in Russian).
[9] V.V. Kim, A.M. Molodets. Programma dlya rascheta volnovykh vzaimodejstvij i termodinamicheskogo sostoyaniya mnogoslojnykh mishenej pri odnomernom udarnom nagruzhenii STAG. // Svidetel'stvo o gosudarstvennoj registratsii programmy dlya EVM № 2016616914. 22 iyunya 2016. (in Russian).
[10] A.M. Molodets, A.G. Golyshev, D.V. Shahrai, D.Yu. Kovalyov. FTT **62**, *1*, 59 (2020). (in Russian).
[11] A.M. Molodets, A.A. Golyshev. FTT **61**, *8*, 1492 (2019). (in Russian).
[12] A.A. Golyshev, V.V. Kim, A.N. Emelyanov, A.M. Molodets. Zhurnal prikladnoj mekhaniki i tekhnicheskoj fiziki **56**, *4*, 92 (2015). (in Russian).
[13] A.V. Pavlenko. V sb.: XIII Mezhdunarodnaya konferentsiya „Zababakhinskie nauchnye chteniya“ 20–24 marta 2017 Snezhinsk, Rossiya. Trudy ZNCh-2017. RFYaTs-VNIITF. (in Russian). https://vniitf.ru/data/images/zst/2017/section_4/13_pavlenko_ru.pdf (2017).
[14] E.K. Cerreta, F.L. Addessio, C.A. Bronkhorst, D.W. Brown, J.P. Escobedo, S.J. Fensin, G.T. Gray III, T. Lookman, P.A. Rigg, and C.P. Trujillo, in Shock Compression of Condensed Matter 2013, edited by W. Buttler, M. Furlanetto, W. Evans (IOP Publishing, Seattle, WA, 2013), Vol. 500, p. 032003.
[15] C.T. Seagle, E. Cottrell, Y. Fei, D.R. Hummer, V.B. Prakapenka. Geophys. Res. Lett. **40**, 5377 (2013).
[16] A.M. Molodets, A.A. Golyshev. Zhurnal tekhnicheskoy fiziki, *9* (91), 1403 (2021). (in Russian).
[17] L.M. Barker, R.E. Hollenbach. J. Appl. Phys. **43**, 4669 (1972).

Translated by I.Mazurov